# ESA Climate Change Initiative Phase-II Sea Surface Temperature

www.esa-sst-cci.org

# Bayesian Cloud Detection for AVHRR SST Retrieval

Claire Bulgin, Chris Merchant, Owen Embury

The Advanced Very High Resolution Radiometer (AVHRR) instrument record spans four decades providing the longest climate data record of sea surface temperature. The majority of AVHRR data are provided at one of two data resolutions: full resolution at 1.1 km in the nadir, and Global Area Coverage (GAC) nominally at 4km resolution. GAC data are an average over four full resolution pixels, but represent the equivalent of fifteen full resolution pixels in the Earth view (five across track by three along track). Cloud detection is a fundamental pre-processing step for sea surface temperature retrieval from satellite data, and critical to the production of datasets appropriate for use in climate studies. It still presents challenges in classifying features such as cloud edges, fog and pixel or sub-pixel cloud, and providing consistent masking under sunglint conditions and at sea-ice edges. We demonstrate here a Bayesian cloud detection scheme applied to both full resolution and GAC resolution data.

## 1. Generating AVHRR Probability Density Functions (PDFs)

Bayesian cloud detection as applied to AVHRR instruments within the SST CCI project uses RTTOV 11.3 to simulate clear-sky conditions. Cloudy observations are represented by empirical PDFs. We calculate these independently from METOP-A full resolution and GAC resolution data spanning 10 years. We construct two-channel spectral PDFs in the visible (0.6 and 0.8 µm), and two and three channel PDFs in the infrared (11, 12 µm and 3.7, 11, 12 µm). We also use a textural PDF based on the local standard deviation in a 3 x 3 pixel window in the 11 µm channel. METOP-A PDFs are used with all AVHRR instruments with 'shifts' in the infrared brightness temperatures applied when the PDFs are read, to make data 'look like' METOP-A.

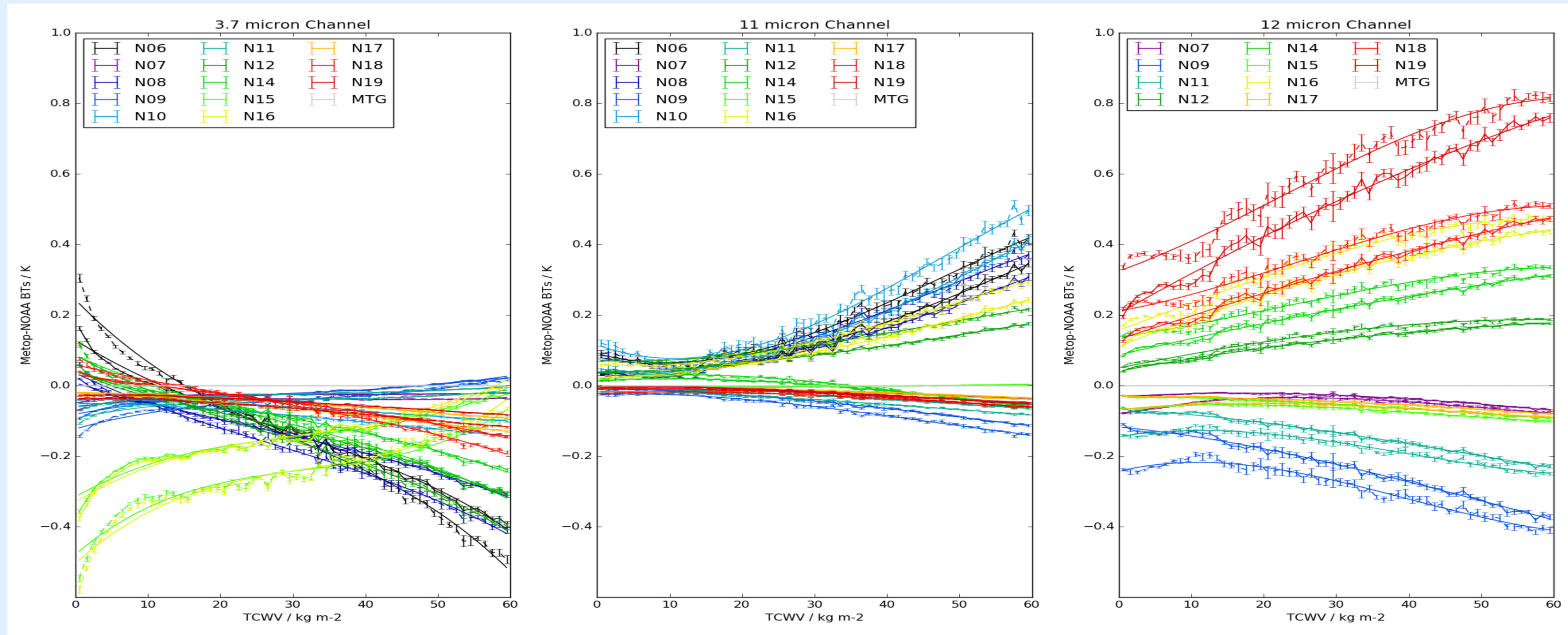


Figure 1: Brightness temperature shifts for the 3.7, 11 and 12 micron channels as a function of total column water vapour, in order to use METOP-A GAC PDFs with other AVHRR instruments. Atmospheric path lengths of 1 and 1.8 are shown, with results interpolated for other path lengths.

## 2. Full Resolution Cloud Detection

Figure 2 shows the Bayesian cloud detection performance compared to the EUMETSAT operational mask for full resolution AVHRR data. The Bayesian algorithm detects (a) more thin cirrus, (b) more clear-sky in the cyclone system and (c) performs well in moderate sunglint. Figure 3 shows day and nighttime SST differences between satellite and in-situ measurements. The Bayesian mask reduces the cold tail of the distribution.

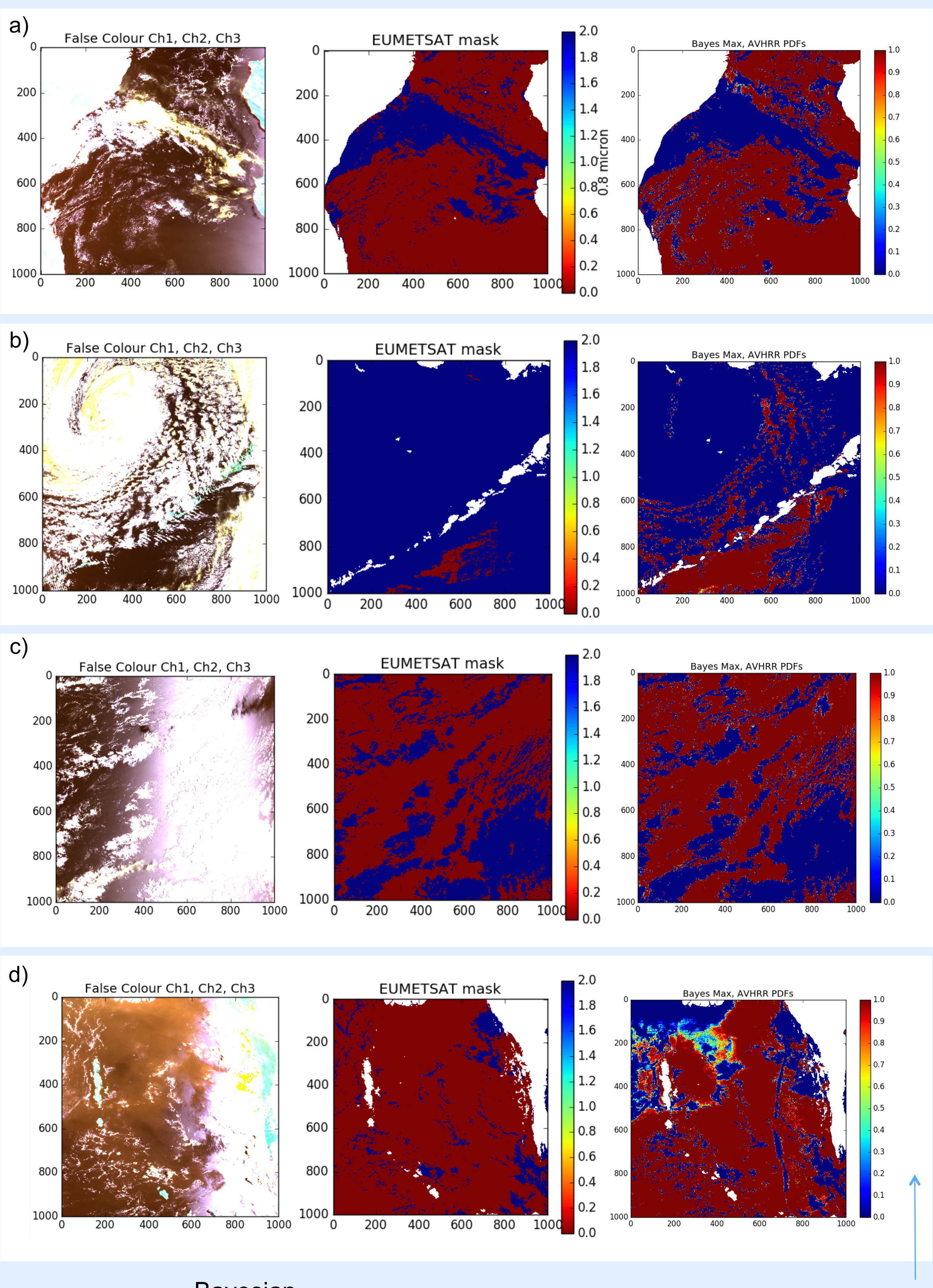


Figure 2: Bayesian cloud detection compared to EUMETSAT cloud detection for: a) bright cirrus clouds, b) cyclone, c) sunglint, d) strong sunglint. Each panel shows a false colour image, the EUMETSAT mask and the Bayesian mask.

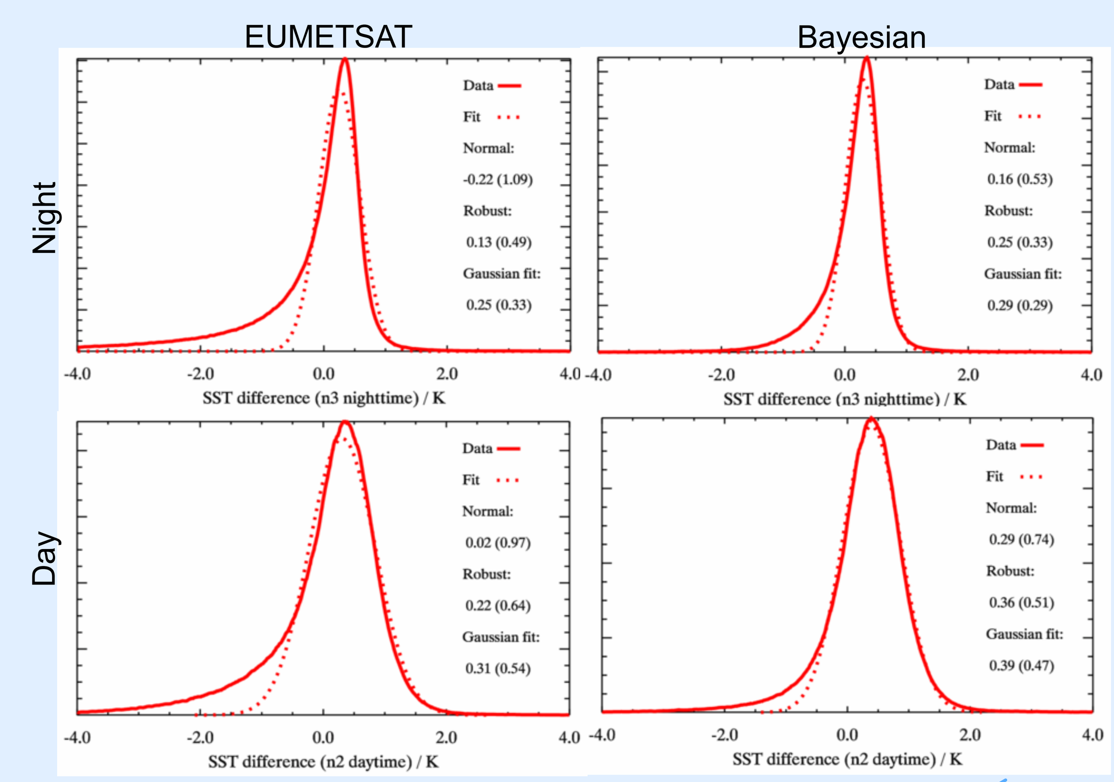


Figure 3: SST differences between satellite retrievals and drifting buoys for nighttime (upper) and daytime (lower) retrievals. Comparisons are made for clear-sky matches defined using the EUMETSAT mask (left) and Bayesian mask (right).

## 3. GAC Resolution Cloud Detection

Figure 4 compares the Bayesian cloud detection against CLAVR-X for a NOAA-14 image, where it correctly identifies more clear-sky pixels under sunglint conditions. Table 1 uses SST validation statistics to quantify cloud mask performance. For most sensors in the series, the Bayesian mask reduces both the differences between the standard deviation and robust standard deviation, indicative of a reduction in cloud contamination in clear-sky matches.

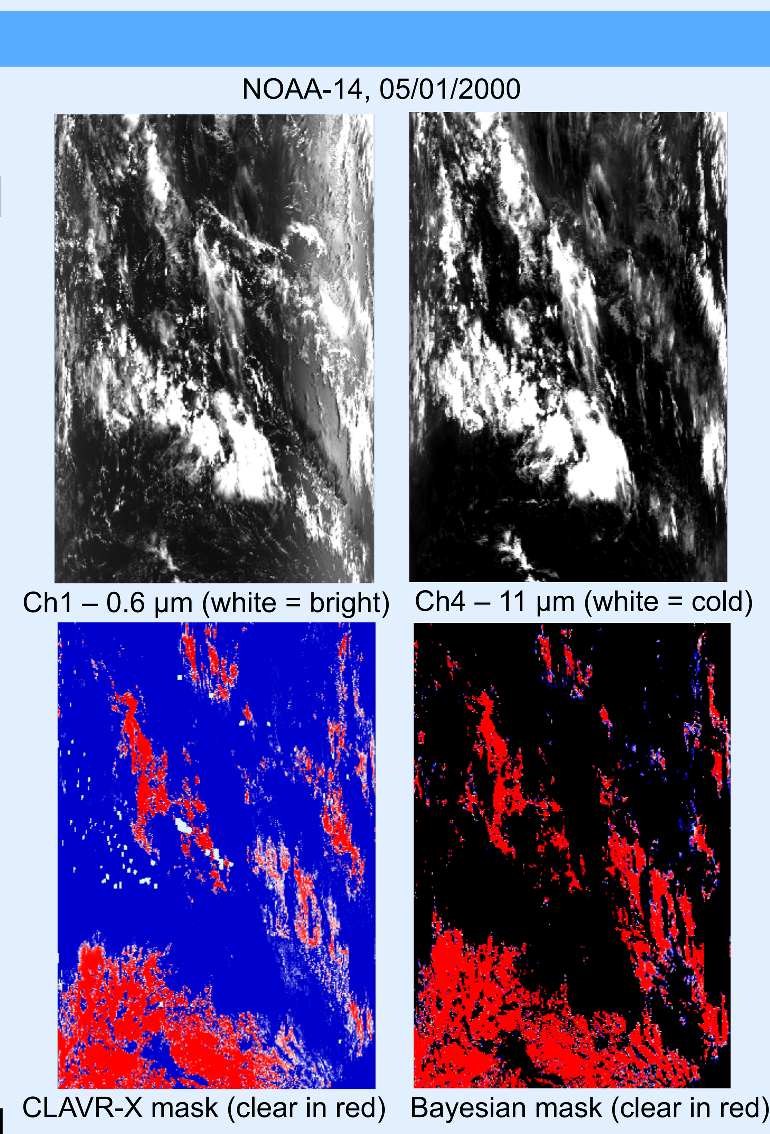


Figure 4: Cloud detection comparison for NOAA-14. Extract shows daytime imagery in a sunglint region, red colour in the cloud masks denotes clear-sky.

| Instrument | Ratio of matches | Ratio of Standard Deviation | Ratio of Robust Standard Deviation |
|---|---|---|---|
| METOP-A | 0.92 | 0.64 | 0.98 |
| NOAA-19 | 0.92 | 0.67 | 0.95 |
| NOAA-18 | 0.88 | 0.7 | 0.98 |
| NOAA-17 | 0.85 | 0.88 | 0.97 |
| NOAA-16 | 0.92 | 0.88 | 1.04 |
| NOAA-15 | 0.82 | 0.89 | 1.007 |
| NOAA-14 | 0.96 | 0.93 | 1.04 |
| NOAA-12 | 1.06 | 0.86 | 0.99 |
| NOAA-11 | 0.79 | 0.88 | 1.004 |
| NOAA-10 | 0.72 | 0.44 | 0.74 |
| NOAA-09 | 0.66 | 0.71 | 0.87 |
| NOAA-08 | 0.74 | 0.89 | 0.80 |
| NOAA-07 | 0.43 | 0.54 | 0.58 |
| NOAA-06 | 0.62 | 0.36 | 0.68 |

Table 1: Ratio (Bayesian/CLAVR-X) of the number of matches and (robust) standard deviation (STD) of satellite/in-situ SST differences. Numbers < 1 in the STD comparisons indicate an improvement.

esa · University of Reading · University of Leicester · National Oceanography Centre, Natural Environment Research Council · Met Office · Norwegian Meteorological Institute · Meteo France, Toujours un temps d'avance · DMI · Brockmann Consult · Space ConneXions